metals

MDPI

Communication

Investigations into the Microstructure and Texture Evolution of Inertia-Friction-Welded Dissimilar Titanium Alloys

Jun Zhou *, Yanquan Wu, Chunbo Zhang, Wu Liang, Rui Li and Feng Qin

Harbin Welding Institute Limited Company, Harbin 150028, China; hwi_wyq@163.com (Y.W.); zhangcbcb@163.com (C.Z.); liangwuweld@163.com (W.L.); 18845618114@163.com (R.L.); banchunqiu@163.com (F.Q.)
* Correspondence: mch_zhoujun@126.com

Abstract: The welded joint of a dissimilar titanium alloy was obtained via inertial friction welding technology. The characteristics of the bonding interface and the microstructure of the welded joint were investigated via optical microscopy, scanning electron microscopy and electron backscattered diffraction. The results show that fine, equiaxed grains and interdiffusion bands of the elements Mo and Sn were formed in the weld zone under the high temperature and plastic deformation of the inertial friction welding. The weld zone and thermo-mechanically affected zone formed $\langle\bar{1}2\bar{1}0\rangle$ α texture and $\langle 111\rangle$ β texture, respectively.

Keywords: titanium alloy; inertia friction welding; microstructure; texture

check for updates

Citation: Zhou, J.; Wu, Y.; Zhang, C.; Liang, W.; Li, R.; Qin, F. Investigations into the Microstructure and Texture Evolution of Inertia-Friction-Welded Dissimilar Titanium Alloys. *Metals* **2023**, *13*, 1575. https://doi.org/10.3390/met13091575

Academic Editor: Francesca Borgioli

Received: 10 May 2023
Revised: 31 July 2023
Accepted: 11 August 2023
Published: 9 September 2023

1. Introduction

Titanium alloys have been widely used in important parts of aero-engines because of their outstanding advantages, such as their light weight, high specific strength, excellent microstructure stability and good plasticity, toughness and high-temperature deformation performance [1]. In addition, the integration components of an aero-engine also represent an important direction of development to further reduce the weight of the engine and improve its structural strength [2,3]. As a solid-state joining method in between these categories, inertia friction welding (IFW) is performed by pressing a non-rotating component into another component that describes a rotating workpiece. The material at the friction interface does not melt but enters a high-temperature plastic state during the IFW process, which can effectively avoid fusion welding defect such as cracking, oxide slag inclusion and poor fusion [4]. In addition, joints produced via IFW can obtain many advantages from the features of the process, like fewer process control parameters, a small heat input, less deformation, a narrow fusion line, better joint performance and high production efficiency [5,6]. At the same time, IFW has become an important manufacturing process for the rotating parts of advanced aero-engines [7]. It can avoid mechanical assembly using bolts or rivets and maintain uniform behavior all over the aero-engine's rotor [8].

Until now, IFW, with its unique welding characteristics, has been especially suitable for welding dissimilar materials, such as dissimilar nickel alloys [9,10], aluminum and magnesium alloys [11], nickel alloys and steel [12], aluminum alloys and steel [13], copper alloys and steel [14], when compared with fusion welding.

Previously, many published works studying the friction welding of dissimilar titanium alloys focused mainly on linear friction welding (LFW), with respect to the welding parameters, the microstructure and the mechanical properties. In the case of LFW, Ballat-Durand, D. [15] and Xavier Boyat et al. [16] analyzed the interfacial characteristics and microstructural changes in linear-friction-welded joints for dissimilar titanium alloys, specifically the β-metastable Ti17 alloy and the near-α Ti6242 alloy. Du et al. [17] further investigated interface microstructural features of a linear-friction-welded joint between TC11 and TC17 titanium alloys. The results showed that the common grains and common grain boundaries were formed simultaneously at the weld interface, and the grain boundary could move between the two materials to form common grains when the crystal orientations on both sides of the weld interface were similar. In a study on the effects of post-weld heat treatment on the fracture toughness of linear-friction-welded joints for TC4 and TC17 alloys, Tao et al. [18] found that thick lamellar and elongated microstructures present higher levels of fracture toughness than fine acicular and equiaxed microstructures. When the surfaces of the parent metal's blocks were not ground, a defect layer could be formed in the welded interface which would reduce the mechanical properties of the dissimilar welded joint for Ti64 and Ti17 alloys, as shown by Garcia et al. [19]. There are few reports on the investigation of IFW in dissimilar titanium alloys [20,21]. TC25G is a new $\alpha + \beta$ high-temperature titanium alloy which can provide long-term service at 550 °C. Compared with the $\alpha + \beta$ titanium alloy, the near-α Ti65 alloy can maintain its tensile strength and demonstrates significant creep resistance at 650 °C. As a material that could potentially be applied in aero-engine compressor components, a dissimilar material joint can satisfy the demands of varying temperature and stress conditions. Therefore, the main goal in the work is to investigate the microstructure and texture evolution of the weld zone during the IFW process of welding dissimilar high-temperature titanium alloys: the $\alpha + \beta$ TC25G alloy, a new $\alpha + \beta$ titanium alloy developed for aerospace applications [22], and the near-α Ti65 alloy.

2. Material and Experiments

The welded joint was obtained by using a home-made HWI-IFW-130B IFW machine developed at Harbin Welding Institute Limited Company, Harbin, China. The material in this study consisted of two billets with the same outer diameter of 150mm and a wall thickness of 20 mm. The $\alpha + \beta$ TC25G and near-α Ti65 alloys were provided in a solution-treated and then aged configuration and as a forging alloy, respectively, and the nominal chemical composition of each alloy is detailed in Table 1. The maximum working temperatures of the TC25G and Ti65 alloys can reach 550 °C and 650 °C, respectively. Based on previous research and an obtained effective welded joint, the IFW process parameters selected in this study were as follows: a rotation speed of 400 r/min, a friction pressure of 50 MPa, a forging pressure of 80 MPa and a moment of inertia of 388 $kg \cdot m^2$. The two dissimilar titanium alloys were welded and then air-cooled. Prior to welding, the welding surfaces of the workpieces were cleaned via turning and alcohol prior to welding. After welding, block samples of $15 \times 10 \times 5$ mm^3 were cut from the welded joint via wire cutting, and a sample coordinate system is shown in Figure 1. Observations of the microstructure and texture were carried out on 10×5 mm^2 surfaces of the extracted samples via optical microscopy (OM), scanning electron microscopy (SEM) and electron backscattered diffraction (EBSD). The polished specimens were etched using an etchant with the following composition: 7 vol.% of hydrofluoric acid, 13 vol.% of nitric acid and 80 vol.% of H_2O. The sample intended for the metallurgical examination was mechanically polished and then etched in the reagent. Another EBSD specimen was prepared utilizing mechanical and vibratory polishing methods.

Table 1. Nominal chemical compositions of TC25G and Ti65 alloys.

Element		Ti	Al	Mo	Nb	Zr	Sn	Si	W	Ta
Wt%	TC25G	Bal	6.60	3.98	-	3.64	1.89	0.21	1.00	-
	Ti65	Bal	5.81	0.50	0.27	3.41	4.16	0.39	0.78	1.02

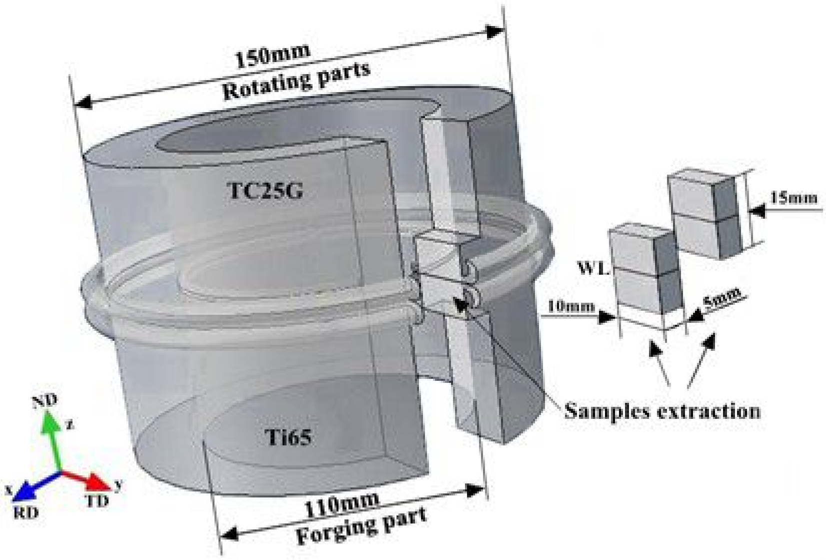

Figure 1. Schematic diagram of block samples.

3. Results and Discussion

The morphology, determined via OM, of the dissimilar IFW joint in different microstructure zones located in the cross-section of the ND-TD plane is shown in Figure 2. The weld zone (WZ), thermo-mechanically affected zone (TMAZ) and base metal (BM) can be easily distinguished according to the differences in their microstructure characteristics, which are due to the different effects of the temperature and plastic deformation of IFW, ranging from the weld interface to the base material on both sides of the welded interface. A heat-affected zone (HAZ) was not found in the inertia-friction-welded joint of dissimilar TC25G + Ti65 titanium alloys compared to the results of previous research [23]. The fusion line is clearly demonstrated within the center of the WZ due to the glaring differences in the microstructural features of the α + β TC25G and α Ti65 alloys. The width of the WZ on both sides of the fusion line is approximately 1.3mm under these welding process parameters. Because of the higher β-transus of the TC25G alloy and its high-temperature resistance compared with the Ti65 alloy, the width of the WZ on the side of the TC25G alloy presents a narrow size and occupies only two-fifths of the WZ. On the contrary, the size of the TMAZ located in the TC25G alloy is obviously wider than on the other side, which can be clearly observed via the transmutative prior α phase. However, similar to a joint [24], the heat-affected zone is not clearly identifiable based on the microstructure and changes in morphology compared with the BM from Figure 2a owing to low energy input. In addition, a typical microstructure in the WZ, as shown in Figure 2b, shows refined, equiaxial β grains when compared with the BM, indicating the occurrence of dynamic recrystallization under the thermo-mechanical coupling affected during the IFW. The typical element distribution across the weld interface was analyzed and is shown in Figure 2c. An interdiffusion band of approximately 20 μm, appearing perpendicular to the weld interface, can be clearly observed via the change in element contents in the transition zone. The results indicated that the interdiffusion process of the elements on both sides of the weld interface is effectively promoted under the high temperature and plastic deformation of IFW.

Based on the above analysis results, the EBSD technique was used to further investigate the phase distribution and crystallographic direction due to the microstructural changes across the joint, as shown in Figure 3, in which the α phase and β phase are indicated in red and blue, respectively. The black lines in Figure 3a represent high-angle grain boundaries (HAGBs) with a misorientation of over 15°, while the white lines represent low-angle grain boundaries (LAGBs) with misorientation values of 2° and 15°. According to the distribution of the grain boundaries' misorientation, as shown in Figure 4, the HAGBs are predominant in the WZ, and the percentage of HAGBs is increased from the TMAZ (approximately 62.5%

on the TC25G side and 65.9% on the Ti65 side, respectively) to the WZ (approximately 79.6% on the TC25G side and 76.3% on the Ti65 side, respectively). The grain boundary distribution in the WZ is more concentrated than that in the TMAZ. The main reason for this is that sufficient dynamic recrystallization occurred in the WZ compared with the TMAZ, resulting from the effects of different thermal–mechanical couplings. As can be seen from Figure 3a, in the case of the as-welded condition, the phase of the TMAZ located on the TC25G side consists of an α phase and a β phase. The percentages of the α phase and β phase are 62.7% and 37.3%, respectively. At the same time, the β phase gradually decreases with an increasing distance from the TAMZ to the fusion line of the WZ. However, in the WZ and TMAZ of the Ti65 alloy side, the microstructure is mainly composed of an α phase (indicated in a red color). The β phase contents in the WZ and TMAZ are only 1.3% and 0.4%, respectively. Therefore, the β phase can be ignored in the WZ and TMAZ of the Ti65 side.

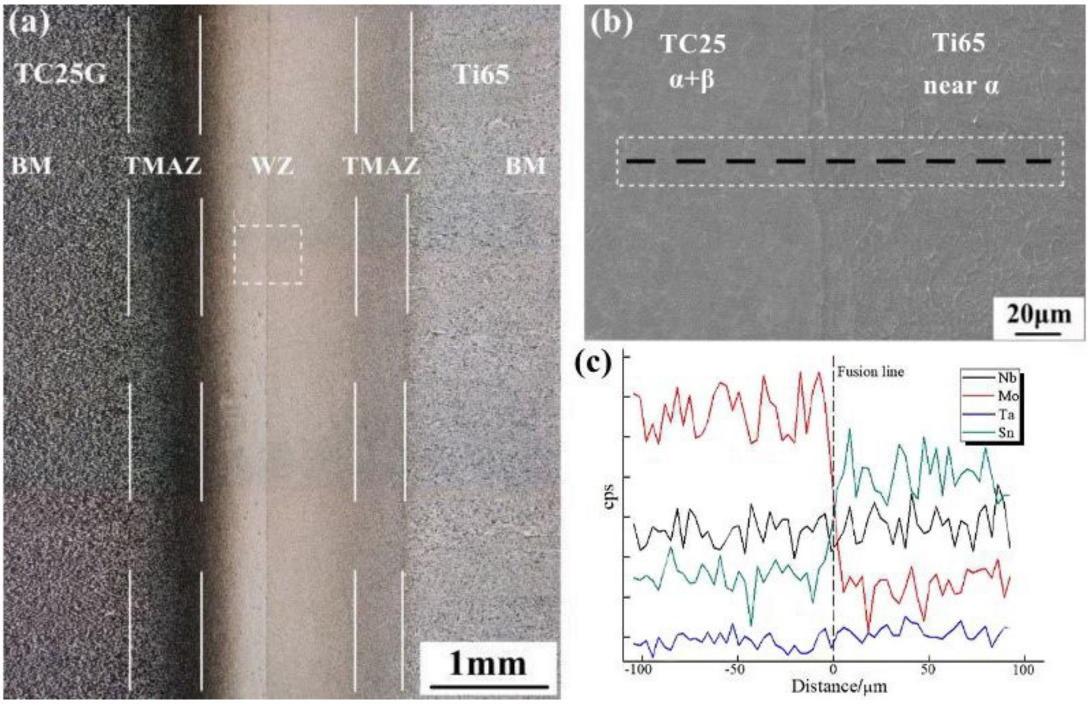

Figure 2. (**a**) Overall view of the cross-section on the joint, image obtained via OM; (**b**) typical microstructure of a weld zone, image obtained via SEM; (**c**) line profile of elemental composition distribution across the weld interface, determined using EDS.

The ND-axis IPF map of the WZ and TMAZ with respect to the crystallographic directions of each grain relative to the normal direction are shown via color codes in Figure 3b. The refined and deformed grains in the WZ and TMAZ, respectively, are shown in Figure 3b according to the size and morphology from the fusion line of the WZ to the TMAZ, and the multifarious crystal orientation relative to the ND is also presented. It can be clearly observed that the major crystallographic directions of more α grains in the WZ are in the $\langle\bar{1}2\bar{1}0\rangle$ direction. At the same time, the orientations of the metastable β grains in the WZ on the TC25G side are mainly concentrated in the $\langle 111\rangle$ direction. The prior α phase and the partial original β grains of the TMAZ on both the TC25G and Ti65 sides are elongated along the direction of the material's flow under the effects of thermal cycling and welding pressure, and the result is that the concentrated crystallographic orientations are formed. Thus, the major orientation of the α grains is concentrated in the $\langle\bar{1}2\bar{1}0\rangle$ direction in the TMAZ of the TC25G side and Ti65 side, and the major orientation of the β grains in the TMAZ on the TC25G side is concentrated in the $\langle 111\rangle$ direction. The α and β phases in the TMAZ show the same crystal orientation as those in the WZ.

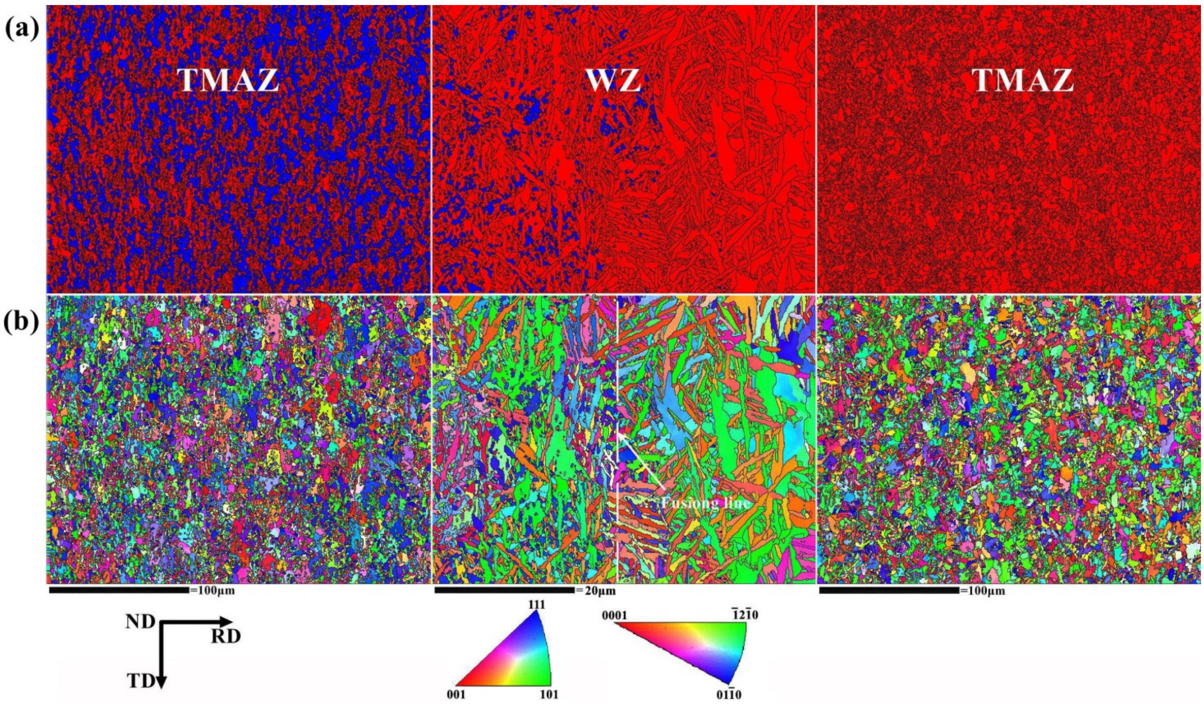

Figure 3. The ND-axis IPF map of the (**a**) α phase and (**b**) β phase, indicated in red and blue, including the WZ and TMAZ on both the TC25G and Ti65 sides.

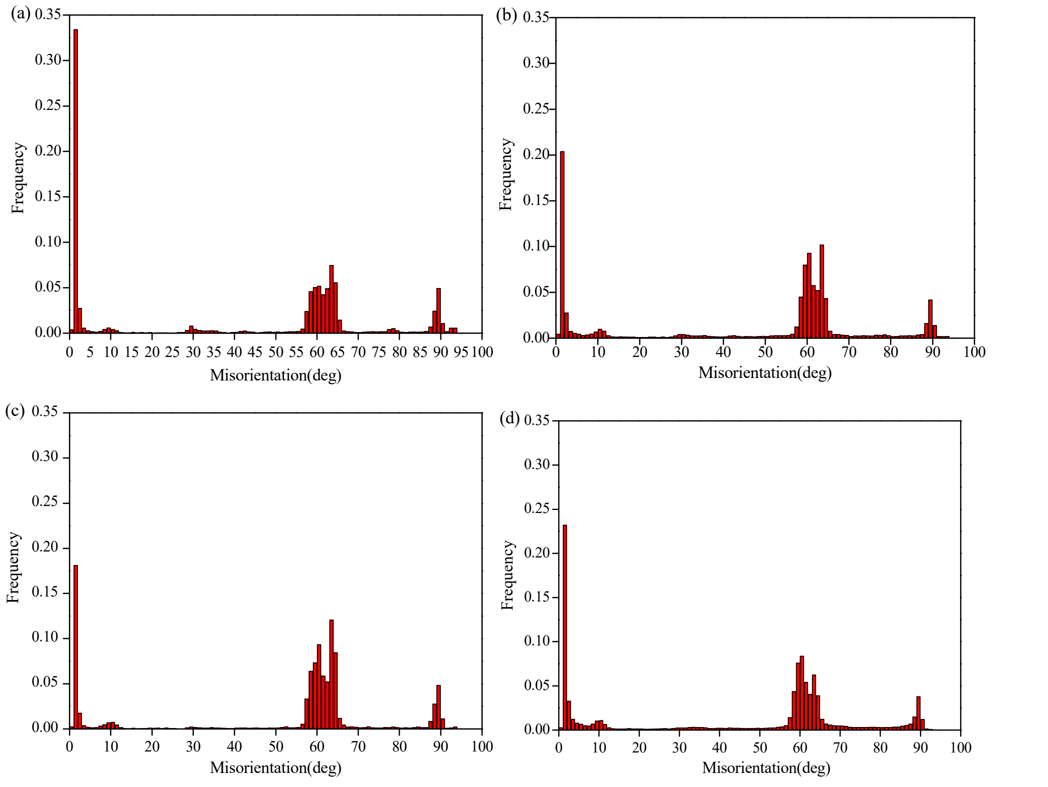

Figure 4. Misorientation distribution of different areas: (**a**) the WZ and (**b**) TMAZ of the TC25G side; (**c**) the WZ and (**d**) TMAZ of the Ti65 side.

In order to further analyze the textures of the α and β phases in the WZ and TMAZ of the welded joint, they are represented by {0001}, {11–20} and {100}, {110}, {111} pole figures, respectively. Figure 5a–d show the pole figures of the α and β phases of the WZ and TMAZ on the TC25G side and Ti65 side, respectively. As can be seen from Figure 5, the {0001} and {11–20} pole figures correspond well with the {110} and {111} in the WZ and TMAZ. Meanwhile, the phenomenon also indicates that the crystallographic orientations of α and β phases exhibit a Burgers orientation relationship. As shown in the {0001} pole figure of Figure 5a,c in the WZ, the maximum intensities are 28.34 and 20.1 times greater, respectively, and the highest density point is distributed at negative 90° from the ND toward the TD. In addition, the TC25G side and Ti65 side of the TMAZ have several high-density points in the {0001}, {11–20} and {111} pole figures. This indicates that there is a sharp texture in the TMAZ.

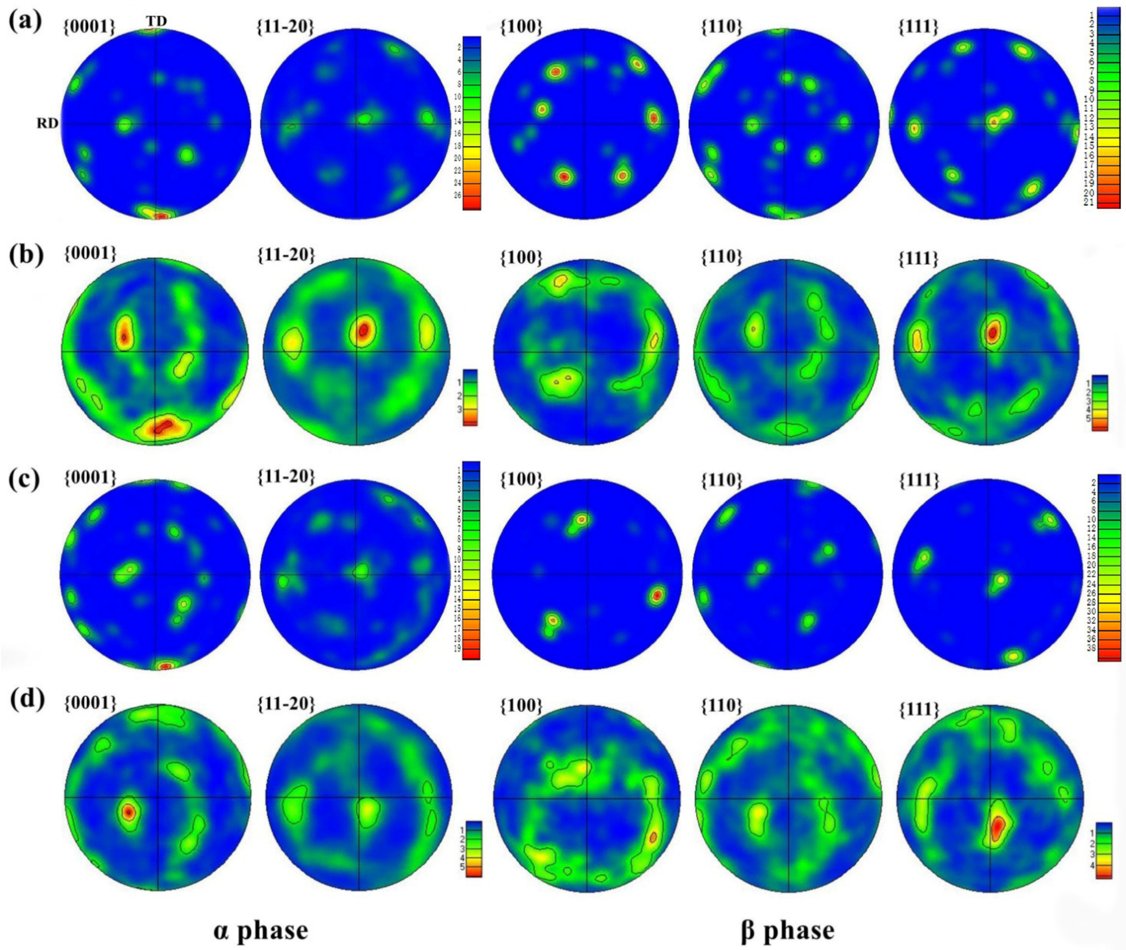

Figure 5. The pole figures of the α and β phases in (**a**) the WZ and (**b**) TMAZ of the TC25G side and (**c**) the WZ of the Ti65 side; (**d**) the pole figures of the α phase in the TMAZ of the Ti65 side.

4. Conclusions

In the present study, the microstructure and texture evolution of a TC25G- and Ti65-alloy joint in a weld zone are systematically investigated. Four conclusions have been reached.

1. TC25G and Ti65 dissimilar titanium alloys have good performance in inertia friction welding, and a high-quality welding interface can be obtained under reasonable welding process parameters.
2. The width of the weld zone and the thermo-mechanically affected zone on the side of the TC25G alloy are narrower and wider compared with the Ti65 alloy side due to the higher β-transus and high temperature resistance of the TC25G alloy.
3. Refined, equiaxial β grains and an interdiffusion band of approximately 25 μm are formed in the weld zone under the high temperature and plastic deformation of IFW.

4. The weld zone and thermo-mechanically affected zone formed a $\langle\bar{1}2\bar{1}0\rangle$ α texture and $\langle 111\rangle$ β texture, respectively.

Author Contributions: J.Z.: review and editing; Y.W.: conceptualization, methodology, and writing—original draft; C.Z.: supervision and writing; W.L.: validation. R.L.: assistance and validation; F.Q.: software and methodology. All authors have read and agreed to the published version of the manuscript.

Funding: This work was funded by the National Key R&D Program of China (no. 2022YFB3404900) and the National Natural Science Foundation of China (no. 52005139).

Data Availability Statement: All the data that support the findings of this study are included within the article.

Conflicts of Interest: The authors declare no conflict of interest.

References

1. Hewitt, J.S.; Davies, P.D.; Thomas, M.J.; Garratt, P.; Bache, M.R. Titanium alloy developments for aeroengine fan systems. *Mater. Sci. Technol.* **2014**, *30*, 1919–1924. [CrossRef]
2. Huang, C.F. Modern aeroengine integral blisk and its manufacturing technology. *Aeronaut. Manuf. Technol.* **2006**, *4*, 94–100.
3. Zhang, H.Y.; Zhang, L.F. Development Overview of Aeroengine Integral Blisk and Its Manufacturing Technology at Home and Abroad. *Aeronaut. Manuf. Technol.* **2013**, *23*, 38–41.
4. Li, W.Y.; Suo, J.D.; Ma, T.J.; Feng, Y.; Kim, K.H. Abnormal microstructure in the weld zone of linear friction welded Ti-6.5Al-3.5Mo-1.5Zr-0.3Si titanium alloy joint and its influence on joint properties. *Mater. Sci. Eng. A* **2014**, *599*, 38–45. [CrossRef]
5. Nicholas, E.D.; Thomas, W.M. A review of friction processes for aerospace applications. *Int. J. Mater. Prod. Technol.* **1998**, *13*, 45–55.
6. Xiao-Ling, D. The Achievements of Advanced Manufacturing Techniques in Aviation and Aerospace Industries. *Int. J. Plant Eng. Manag.* **2012**, *3*, 145–152.
7. Attallah, M.M. Welding and Joining of Aerospace Materials | | Inertia friction welding (IFW) for aerospace applications. *Weld. Join. Aerosp. Mater.* **2012**, *4*, 25–74.
8. Sol, I.D.; Rivero, A.; de Lacalle, L.N.L.; Gamez, A.J. Thin-Wall Machining of Light Alloys: A Review of Models and Industrial Approaches. *Materials* **2019**, *12*, 2012. [CrossRef]
9. Senkov, O.N.; Mahaffey, D.W.; Semiatin, S.L. Effect of process parameters on process efficiency and inertia friction welding behavior of the superalloys LSHR and Mar-M247. *J. Mater. Process. Technol.* **2017**, *250*, 156–168. [CrossRef]
10. Tiley, J.S.; Mahaffey, T.; Alamb, D.W. Strengthening mechanisms in an inertia friction welded nickel-base superalloy. *Mater. Sci. Eng. A* **2016**, *662*, 26–35. [CrossRef]
11. Guo, W.; You, G.; Yuan, G.; Zhang, X. Microstructure and mechanical properties of dissimilar inertia friction welding of 7A04 aluminum alloy to AZ31 magnesium alloy. *J. Alloys Compd.* **2017**, *695*, 3267–3277. [CrossRef]
12. Ding, Y.H.; You, G.Q.; Wen, H.Y.; Li, P.; Tong, X.; Zhou, Y. Microstructure and mechanical properties of inertia friction welded joints between alloy steel 42CrMo and cast Ni-based superalloy K418. *J. Alloys Compd.* **2019**, *803*, 176–184. [CrossRef]
13. Ma, H.; Qin, G.L.; Geng, P.H.; Wang, S.; Zhang, D. Microstructural characterisation and corrosion behaviour of aluminium alloy/steel hybrid structure produced by friction welding. *J. Manuf. Process.* **2021**, *61*, 349–356. [CrossRef]
14. Wu, W.; Zhu, L.Y.; Wu, G.F.; Bin Xu, H. Study on Performance of Inertia Radial Friction Welding of Copper-Alloy to 35CrMnSi Steel. *Adv. Mater. Res.* **2011**, *291–294*, 968–974. [CrossRef]
15. Ballat-Durand, D.; Bouvier, S.; Risbet, M.; Pantleon, W. Through analysis of the microstructure changes during linear friction welding of the near-α titanium alloy Ti-6Al-2Sn-4Zr-2Mo (Ti6242) towards microstructure optimization. *Mater. Charact.* **2019**, *151*, 38–52. [CrossRef]
16. Boyat, X.; Ballat-Durand, D.; Marteau, J.; Bouvier, S.; Favergeon, J.; Orekhov, A.; Schryvers, D. Interfacial characteristics and cohesion mechanisms of linear friction welded dissimilar titanium alloys: Ti-5Al-2Sn-2Zr-4Mo-4Cr(Ti17) and Ti-6Al-2Sn-4Zr-2Mo(Ti6242). *Mater. Charact.* **2019**, *158*, 109942. [CrossRef]
17. Du, S.; Gao, M.; Xu, W.; Wang, X. Study on Interface of Linear Friction Welded Joint Between TC11 and TC17 Titanium Alloy. *Acta Metall. Sin.* **2019**, *55*, 885–892.
18. Tao, B.; Li, Q.; Zhang, Y.; Zhang, T.; Liu, Y. Effects of post-weld heat treatment on fracture toughness of linear friction welded joint for dissimilar titanium alloys. *Mater. Sci. Eng. A* **2015**, *634*, 141–146. [CrossRef]
19. Garcia, J.M.; Esin, V.A.; Morgeneyer, T.F. Strength, fatigue strength and toughness of dissimilar Ti17–Ti64 linear friction welded joints: Effect of soft surface contamination and depletion of α precipitates. *Mater. Sci. Eng. A* **2020**, *799*, 139989. [CrossRef]
20. Zhanglong, Z.; Xuyang, S.; Lanchuan, C.; Wenxin, X.; Zekun, Y.; Hongzhen, G. The effect of isothermal deforming on the microstructure and property of inertial friction welding IMI834/Ti6246 dual titanium alloy. *Rare Met. Mater. Eng.* **2020**, *49*, 2388–2392.

21. He, J.H.; Zhang, T.C.; He, S.C. Research of Microstructure and Mechanical Properties of Ti600/TC17 Inertia Friction Welding Joints. *J. Mech. Eng.* **2017**, *53*, 95–100. [CrossRef]
22. Liu, Y.H.; Zhao, Z.B.; Zhang, C.; Wang, Q.; Sun, H.; Li, N. Thermal and mechanical induced texture evolution of inertia friction welding in α + β titanium alloy. *Mater. Lett.* **2020**, *277*, 128329. [CrossRef]
23. Wu, Y.Q.; Zhang, C.B.; Zhou, J.; Liang, W.; Li, Y. Analysis of the Microstructure and Mechanical Properties during Inertia Friction Welding of the Near-α TA19 Titanium Alloy. *Chin. J. Mech. Eng.* **2020**, *33*, 13. [CrossRef]
24. Wen, G.D.; Ma, T.J.; Li, W.Y.; Wang, S.Q.; Guo, H.Z.; Chen, D.L. Strain-controlled fatigue properties of linear friction welded dissimilar joints between Ti-6Al-4V and Ti-6.5Al-3.5Mo-1.5Zr-0.3Si alloys. *Mater. Sci. Eng. A* **2014**, *612*, 80–88. [CrossRef]